Title	A braided stent becomes flattened inside a curved catheter tube: A micro-CT imaging study
Author(s)	Shigematsu, Taiki; Otani, Tomohiro; Tomotake, Shotaro et al.
Citation	Bio-Medical Materials and Engineering. 2020, 31(6), p. 373-380
Version Type	AM
URL	https://hdl.handle.net/11094/88323
rights	
Note	

A Braided Stent Becomes Flattened Inside a Curved Catheter Tube:

Micro-CT Imaging

Taiki Shigematsu[a,b], Tomohiro Otani[a], Shotaro Tomotake[c], Shunya Shiozaki[a], Shigeo Wada[a]

[a]*Department of Mechanical Science and Bioengineering, Graduate School of Engineering Science, Osaka University, Toyonaka, Osaka, 560-8531, Japan*
[b]*Global Center for Medical Engineering and Informatics, Osaka University, Suita, Osaka, 565-0871, Japan*
 [c]*Department of Systems Science, School of Engineering Science, Osaka University, Toyonaka, Osaka, 560-8531, Japan*

Corresponding author: Tomohiro Otani,
Department of Mechanical Science and Bioengineering, Graduate School of Engineering Science, Osaka University, Toyonaka, Osaka, 560-8531, Japan.
TEL: +81-6-6850-6174
E-mail: otani@me.es.osakau.ac.jp

Abstract

BACKGROUND: The braided stent is a widely accepted endovascular treatment device consisting of woven metal wires. One of open issues for the braided stent is the stent flattening phenomena when deploying into highly curved arteries. Although recent computational study highlighted that the mechanical state of the stent inside the catheter before the deployment plays an essential role in causing stent flattening, there is no experimental observation for the stent inside the curved catheter.

OBJECTIVE: We investigated braided stent shapes in curved catheter tubes with various curvatures by micro-computed tomography (CT).

METHODS: A braided stent was deployed into catheter tubes and set in rectangular cases with constant curvature. The three-dimensional shape of the stent was imaged by micro-CT, and its cross-sectional flatness was quantitatively assessed.

RESULTS: Stent flattening occurred in cases of high curvatures of the outer side of the tube curvature, and the degree of flatness increased with increasing tube curvature. This demonstrates that stent flattening can be caused inside the highly curved catheter before deployment.

CONCLUSIONS: This preliminary and first observational report provides new insight into the mechanism of stent flattening and emphasizes the importance of the geometrical and mechanical state of the stent inside the catheter.

1. Introduction

The braided stent is a widely accepted endovascular device and has recently attracted interest for cerebral aneurysm treatment as a self-expanding intracranial stent. The braided stent is a simple cylindrical structure that consists of woven metal wires (Fig. 1(a)) and is deployed in parent arteries of cerebral aneurysms via a catheter assisted by guidewire. The stent is mainly used for assisting endovascular coiling to prevent coil protrusion from aneurysms [1,2] and as a flow-diverter to isolate the aneurysm from parent arteries [3,4].

A critical issue of the braided stent is technical difficulties of its deployment compared to other kinds of stents [5–7], which may be due to the relatively weak radial force for expansion [5]. These difficulties may lead to the inappropriate stent expansion reported in existing studies [7,8]. Stent flattening is a fatal problem as observed in inappropriate stent expansion patterns during deployment into highly tortuous arteries, in which the braided stent cross-section becomes flattened in the midsection of the arterial curve [8,9]. These experimental observations suggest that the bending deformation of the stent in the curved arteries is an essential factor to cause stent flattening. However, the braided stent, which is fully expanded, rarely becomes flattened even under a large bending deformation (Fig. 1(b)). This fact highlights the necessities to deeply understand the mechanical characteristics of the braided stent to interpret the stent flattening mechanism.

Mechanical characteristics of the braided stent has been paid much attentions especially in last two decades since the braided stent became widely accepted in clinical practice. Several theoretical approaches modeled the braided stent as an assembly of helical coils and estimated the radial force for stent expansion [10–13]. Computational approaches are also promising ones for estimating apparent stiffness of the braided stent, such as axial and flexural rigidities, with considering material nonlinearities and viscoelastic properties of stent wires [14–21]. In particular, recent computational study [22] illustrated that the

mechanical states of the braided stent inside the catheter before deployment and its transition during deployment play an important role to cause the stent flattening. Based on these findings, we hypothesize that the geometric constraints and radial compression by the catheter may be essential to the stent flattening initiated inside the curved catheter before deployment. However, there are no reports that observe the stent shape inside the curved catheter, to our knowledge. Understanding of the three-dimensional (3D) stent shapes in a curved catheter may provide valuable references for further consideration of the stent flattening mechanism.

The present study investigates braided stent shapes in a curved catheter tube with various curvatures by micro-computed tomography (CT). For this aim, we developed an experimental setup to image the 3-D braided stent and quantitatively evaluated the flatness of the stent cross-sections. Section 2 shows an experimental setup of the 3-D stent shape imaging and evaluation of its cross-sectional flatness. The results and their implications are briefly illustrated in Section 3 and Section 4 notes the conclusions.

2. Materials and Methods

2.1. Experimental setup

An experimental setup using micro-CT imaging was developed to image the 3-D braided stent shape in curved catheter tubes. The braided stent consisted of 32 Co-Cr wires, and two Pt wires with a diameter of 40μm (Fig. 1), in which the stent diameter was 5 mm (fully expanded state) for a vascular reconstruction device (VRD) (bare braided material, not the products, provided by Allm Inc., Tokyo, Japan). The stent was deployed into the catheter tube (CNC-3/5H, ACCESS Technologies Inc., IL, USA) with a diameter of 1mm (Fig. 2(a)). The catheter tube with the stent was mounted in a groove in a fixing jig constructed by a 3-D printer OBJECT30 Pro (Stratasys Ltd., MN, USA) with Vero Clear material (RGD810) (Fig. 2(b)). The shape of the groove is rectangular with a width of 1.0 mm and

depth of 1.0 mm. Along the length of the groove, the groove is straight but partially curved with constant length (6.28 mm) and curvatures (0, 0.1, 0.16, 0.25, and 0.33 mm^{-1}) in the middle. The range of the curvature is consistent with those of the actual internal carotid arteries [23]. We defined the centerline coordinate S with $S = 0$ at the midpoint of the curved part along the centerline of the groove.

2.2. micro-CT imaging

The braided stent with a curved catheter tube was imaged using an in-house cone-beam micro-CT scanner (Fig.2(c)). In this scanner, the X-ray source XWT-160TC (X-RAY WorX GmbH, Germany) and flat panel C7942CA-22 (Hamamatsu Photonics, Inc., Japan) were aligned on the horizontal table in a radiation shielding room. The image target was placed vertically on a rotation stage (ALZ-115-E1P, Chuo precision industrial Co., Ltd., Japan) between the X-ray source and flat panel. In the projection images, the pixel size was 8.6 µm×8.6 µm and the number of pixels was 1120×1172. The CT scanning parameters were as follows: the electric voltage was 90 kV, the electric power was 7 W, the total rotation was 360° with a 0.3° rotation step and the exposure time in each angle was 2 seconds. The CT images were output from all projection images by the method of [24] (Fig.2(d)) and the 3-D stent shape was extracted from the CT images by Amira 5.5 (Thermo Fisher Scientific, Inc., MA, USA) considering the ring and metal artifacts and finally exported as a 3-D tiff image file format (Fig.2(e)).

2.3. Evaluations

To quantify stent flattening, we defined the flatness ratio φ of the stent cross-section. From the 3-D images of the stents, 2-D cross-sectional images were extracted along the centerline of the rectangular grooves (e.g., Fig. 3 (b)). The stent shapes on the cross-sections were approximated as an ellipsoid and evaluated by a gyration tensor $\mathbf{G} \in \square^{2 \times 2}$. Its component G_{ij} is defined as

$$G_{ij} = \frac{1}{N}\sum_{k=1}^{N} x_i^k x_j^k \, , \tag{1}$$

where **x** is the position vector of the stent wire pixels in the cross-sectional images and N is number of those pixels. The length of longer and shorter axes of the ellipsoid, a and b, can be calculated from the eigenvalues and corresponding eigenvectors of **G**. Using a and b, the flatness ratio φ ($0 \leq \varphi \leq 1$) of the stent cross-section is given by

$$\varphi = \left| \frac{a-b}{a+b} \right| . \tag{2}$$

φ will be 0 when the stent shape is a circle and will be close to 1 when flattened.

3. Results and Discussion

3.1. Stent cross-section flatness

Figure 3 shows a 3-D shape of the braided stent in the catheter tube with the curvature of 0.25 mm^{-1} reconstructed from micro-CT images. Representative stent cross-sections along the centerline at $S = 0, \pm 2$, and ± 4 mm are also included in Fig. 3(b). The stent cross-sections were flattened in the midsection of the curved part and the degree of flattening became gradually modest from the midsection to both ends (Fig. 3(b)). At the flattened part ($S = 0$ mm), the stent cross-sections at the outer side of the tube curvature became concave and the wires tended to concentrate on the outer side (Fig. 3(b) $S = 0$ mm and (c)).

Stent flattening were quantitatively assessed with five patterns of curvatures using the flatness ratio defined in Section 2.3. The flatness ratio of the stent along the centerline of the groove is illustrated in Fig. 4(left). Although the flatness ratio was constantly zero in the straight case (curvature = 0 mm^{-1}), it gradually increased with increasing curvatures and approached 0.8 for the highest curvature. From the

snapshots (Fig. 4(right)), the stent cross-section apparently became flattened when the curvature was 0.25 mm^{-1} or greater. Figure 5 summarizes the maximum flatness ratio of the braided stent in the curved catheter tubes with various curvatures. The maximum flatness ratio monotonically increased with increasing curvature and reached 0.8.

3.2. Implications for stent flattening mechanisms

The observations of this study illustrate stent flattening in the catheter tube with high curvatures. This result demonstrates that the stent flattening can be caused not only during the deployment process, but also before the deployment process when the stent is inside the catheter. This observation supports our hypothesis that radial compression and geometric constraints by the catheter are essential factors that can cause stent flattening. Because the catheter wall is significantly stiffer than the braided stent, the braided stent is compressed in radial directions and its expansion is geometrically constrained in the catheter. Although the association between stent flattening inside the catheter and that inside the arteries is not clear, further investigation of the braided stent mechanics under these mechanical conditions may be valuable to deepening the understanding of the stent flattening mechanism.

In general, bending buckling of cylindrical tube is caused at the inner side of tube curvature, c.f., [25]. However, the stent cross-sections became concave at the outer side of the tube curvature. Because the stent wires do not strictly constrain each other and the wires could slide with increasing tube curvatures, this finding suggests that the braided stent has different mechanical characteristics compared to typical continuum material tube.

3.3. Limitations

This study aims to investigate a 3-D braided stent shape under radial compression and geometric constraints, and the preliminary observations conducted have differences in the experimental protocol from clinical situation. Thus, these differences give rise to mainly three limitations to consider the braided stent flattening in clinical practice. First, the guidewire, which is commonly set in the catheter to assist stent deployment, was not considered because the guidewire causes a severe metal artifact in the CT images making it difficult to segment the stent outlines from the images. The guidewire in the catheter acts as the geometric constraints on the braided stent, and thus this constraint may affect the stent behaviors inside the catheter in a clinical situation. Second, the diameter of the catheter tube used in this study was larger than the catheter used in cerebrovascular treatment, owing to difficulties of setting the braided stent in the catheter tube with a small diameter. Although stent flattening was observed in the curved tubes in this study, the catheter diameter might be an influential factor causing braided stent flattening. Third, we considered the stent flattening in 2-D curved catheter with no torsion, as idealized condition, whereas the actual arteries contain 3-D complexity (*e.g.*, torsion). Further consideration of the actual arterial shape might provide more precise knowledge of the flattening mechanism.

4. Conclusions

The present study investigated braided stent shapes in the curved catheter tubes with various curvatures. An experimental setup to image the 3-D braided stent shapes in the curved tubes was developed with using a micro-CT scanner and the flatness of the stent cross-sections with different catheter curvatures were quantitatively evaluated. Stent flatness was observed in the curved catheter tubes and the degree of flatness increased with increasing catheter curvatures. This finding highlights that the stent flattening can occur inside the curved catheter at the curvature where the flattening does not occur in the case of the expanded

stents. This fact suggests that the mechanical characteristics of braided stent in clinically-reasonable situations (inside the catheter) should be considered, whereas the mechanical characteristics of stents has been investigated usually at fully expanded state. In addition, the stent cross-section became flattened and the concave shape at the outer side of the tube curvature. This implies that the braided stent mechanics cannot be directly interpreted by typical continuum material tube mechanics.

This study demonstrates that stent flattening can occur inside the catheter even before deployment into the curved arteries. The preliminary, but first observation report here provides new insight into the mechanisms of stent flattening and would be helpful for designing the stent shape and deployment protocol.

References

[1]   Kis B, Weber W, Berlit P, Kühne D. Elective treatment of saccular and broad-necked intracranial aneurysms using a closed-cell Nitinol Stent (Leo). Neurosurgery 2006;58:443–50.

[2]   Piotin M, Blanc R, Spelle L, Mounayer C, Piantino R, Schmidt PJ, et al. Stent-Assisted Coiling of Intracranial Aneurysms. Stroke 2009;41:110–5.

[3]   Brinjikji W, Murad MH, Lanzino G, Cloft HJ, Kallmes DF. Endovascular treatment of intracranial aneurysms with flow diverters: A meta-analysis. Stroke 2013;44:442–7.

[4]   Becske T, Kallmes DF, Saatci I, McDougall CG, Szikora I, Lanzino G, et al. Pipeline for uncoilable or failed aneurysms: Results from a multicenter clinical trial. Radiology 2013;267:858–68.

[5]   Lubicz B, Collignon L, Raphaeli G, Pruvo JP, Bruneau M, De Witte O, et al. Flow-diverter stent for the endovascular treatment of intracranial aneurysms: A prospective study in 29 patients with 34 aneurysms. Stroke 2010;41:2247–53.

[6]   Lv X, Li Y, Jiang C, Yang X, Wu Z. Potential advantages and limitations of the Leo stent in endovascular treatment of complex cerebral aneurysms. Eur J Radiol 2011;79:317–22.

[7]   Krischek Ö, Miloslavski E, Fischer S, Shrivastava S, Henkes H. A comparison of functional and physical properties of self-expanding intracranial stents. Minim Invasive Neurosurg 2011;54:21–8.

[8]   Ebrahimi N, Claus B, Lee CY, Biondi A, Benndorf G. Stent conformity in curved vascular models with simulated aneurysm weeks using Flat-Panel CT: An in vitro study. Am J Neuroradiol 2007;28:823–9.

[9]   Valdivia y Alvarado M, Ebrahimi N, Benndorf G. Study of conformability of the new LEO PLUS stent to a curved vascular model using flat-panel detector computed tomography (DynaCT). Neurosurgery 2009;64:130–4.

[10]   Jedwab MR, Clerc CO. A study of the geometrical and mechanical properties of a self-expanding metallic stent--theory and experiment. J Appl Biomater 1993;4:77–85.

[11]   Wang R, Ravi-Chandar K. Mechanical response of a metallic aortic stent - Part I: Pressure-diameter relationship. J Appl Mech Trans ASME 2004;71:697–705.

[12]   Wang R, Ravi-Chandar K. Mechanical Response of a Metallic Aortic Stent—Part II: A Beam-on-Elastic Foundation Model. J Appl Mech 2004;71:706.

[13]   Moon T, Hong D, Chun HJ, Lee KB. Analytical models for predicting mechanical properties of mesh-type self-expandable metal stents with cover membrane. Curr Appl Phys 2009;9:92–100.

[14]   Kim JH, Kang TJ, Yu WR. Mechanical modeling of self-expandable stent fabricated using braiding technology. J Biomech 2008;41:3202–12.

[15]   Zhao S, Liu X (Cheryl), Gu L. The Impact of Wire Stent Fabrication Technique on the Performance of Stent Placement. J Med Device 2012;6:011007.

[16]   Frost M, Sedlák P, Kruisová A, Landa M. Simulations of self-expanding braided stent using macroscopic model of NiTi shape memory alloys covering R-Phase. J Mater Eng Perform 2014;23:2584–90.

[17]   Ni XY, Pan CW, Gangadhara Prusty B. Numerical investigations of the mechanical properties of a braided non-vascular stent design using finite element method. Comput Methods Biomech Biomed Engin 2015;18:1117–25.

[18]   Alherz AI, Tanweer O, Flamini V. A numerical framework for the mechanical analysis of dual-layer stents in intracranial aneurysm treatment. J Biomech 2016;49:2420–7.

[19]   Shanahan C, Tofail SAM, Tiernan P. Viscoelastic braided stent: Finite element modelling and validation of crimping behaviour. Mater Des 2017;121:143–53.

[20]   Fu W, Cheng G, Yan R, Qiao A. Numerical investigations of the flexibility of intravascular braided stent. J Mech Med Biol 2017;17:1750075.

[21]   Fu W, Xia Q, Yan R, Qiao A. Numerical investigations of the mechanical properties of braided vascular stents. Biomed Mater Eng 2018;29:81–94.

[22]   Shiozaki S, Otani T, Fujimura S, Takao H, Wada S. Computational modeling of braided-stent deployment for interpreting the mechanism of stent flattening. Int J Numer Method Biomed Eng 2020, online first.

[23]   Piccinelli M, Bacigaluppi S, Boccardi E, Ene-Iordache B, Remuzzi A, Veneziani A, et al. Geometry of the Internal Carotid Artery and Recurrent Patterns in Location, Orientation, and Rupture Status of Lateral Aneurysms: An Image-Based Computational Study. Neurosurgery 2011;68:1270–85.

[24]   Feldkamp LA, Davis LC, Kress JW. Practical cone-beam algorithm. J Opt Soc Am A 1984;1:612.

[25]   Brazier LG. On the Flexure of Thin Cylindrical Shells and Other "Thin" Sections. Proc R Soc A Math Phys Eng Sci 1927;116:104–14.

Figure captions

Figure 1: Braided stent that consists of 32 Co-Cr wires and two Pr wires (fully expanded (a) and bent by hand (b)).

Figure 2: Experimental setup: (a) The braided stent was packed in the catheter tube; (b) fixing jig; (c) in-house micro-CT scanner; (d) representative raw image file output from the micro-CT scan; and (e) edited image file with eliminating artifacts.

Figure 3: (a) Braided stent shape in the curved catheter tube with a curvature of 0.25 mm^{-1}. (b) Stent cross-sections at S = -4, -2, 0, 2, and 4 mm. (c) Cutaway view of the braided stent (cut at S = 0 mm in (a)).

Figure 4: The flatness ratio of the stent cross-sections at the catheter curvatures is 0 (black), 0.1 (blue), 0.16 (green), 0.25 (yellow), and 0.33 mm^{-1} (pink) (left) and images of each stent cross-sections at the midsection (right). The region between the two dashed lines corresponds to the curved parts of the catheter tubes.

Figure 5: Maximum flatness ratio of the braided stent cross-sections in the curved catheter with various curvatures.
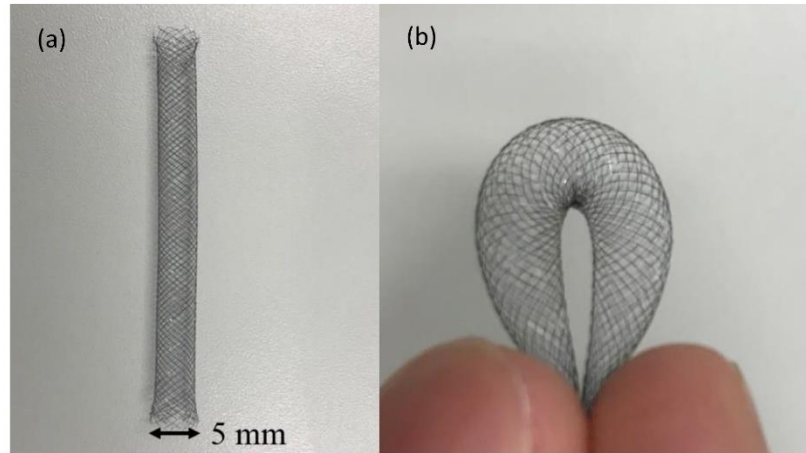
Figure 1: Braided stent that consists of 32 Co-Cr wires and two Pr wires (fully expanded (a) and bent by hand (b)).
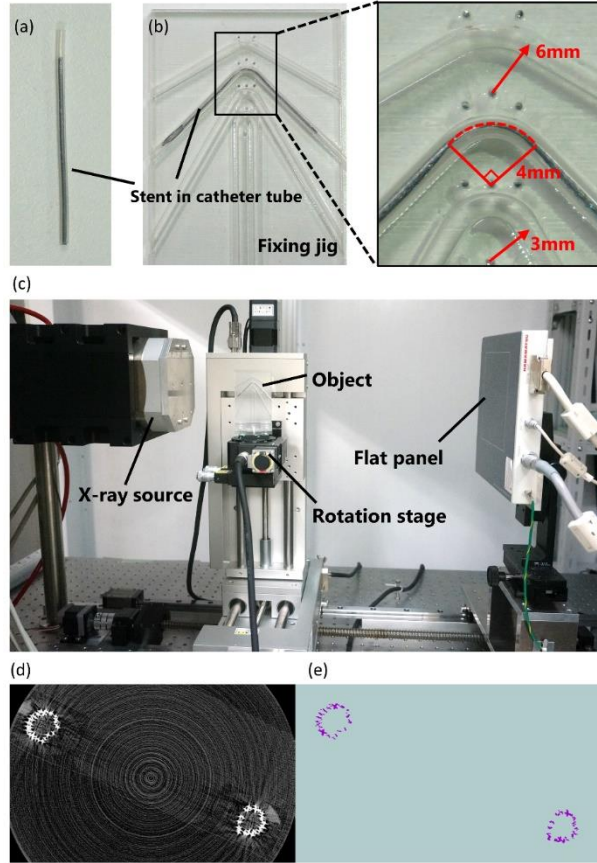
Figure 2: Experimental setup: (a) The braided stent was packed in the catheter tube; (b) fixing jig; (c) in-house micro-CT scanner; (d) representative raw image file output from the micro-CT scan; and (e) edited image file with eliminating artifacts.
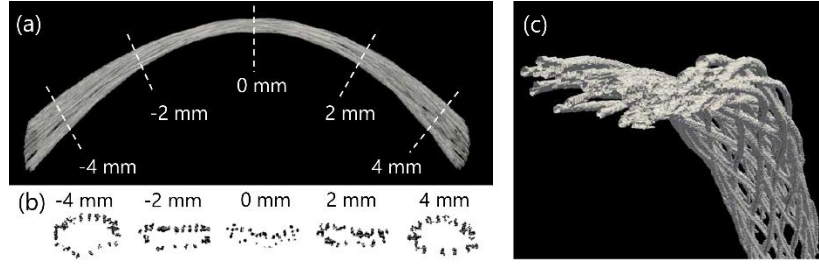
Figure 3: (a) Braided stent shape in the curved catheter tube with a curvature of 0.25 mm^{-1}. (b) Stent cross-sections at $S = $ -4, -2, 0, 2, and 4 mm. (c) Cutaway view of the braided stent (cut at $S = 0$ mm in (a)).
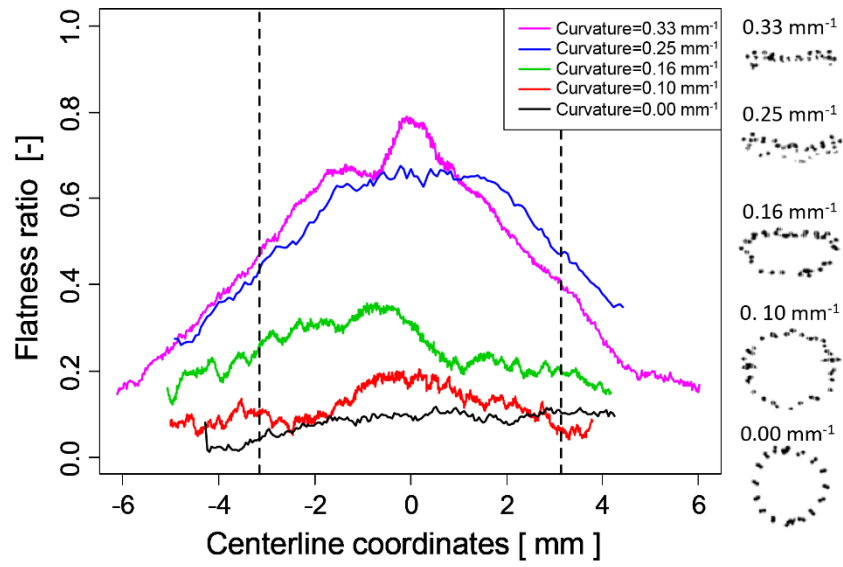
Figure 4: The flatness ratio of the stent cross-sections at the catheter curvatures is 0 (black), 0.1 (blue), 0.16 (green), 0.25 (yellow), and 0.33 mm^{-1} (pink) (left) and images of each stent cross-sections at the midsection (right). The region between the two dashed lines corresponds to the curved parts of the catheter tubes.
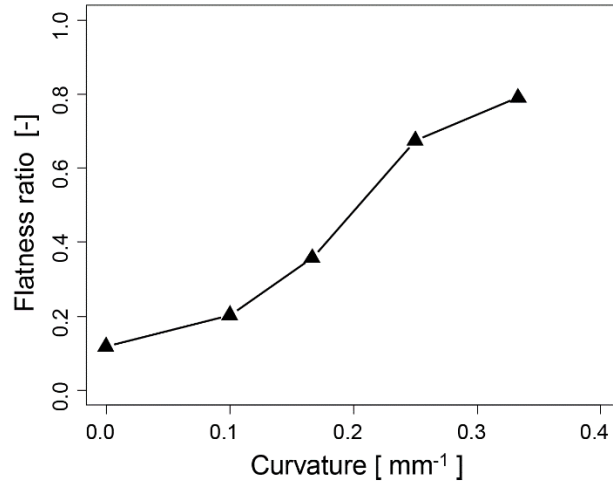
Figure 5: Maximum flatness ratio of the braided stent cross-sections in the curved catheter with various curvatures.